

Dalton Transactions

Accepted Manuscript



This is an *Accepted Manuscript*, which has been through the Royal Society of Chemistry peer review process and has been accepted for publication.

Accepted Manuscripts are published online shortly after acceptance, before technical editing, formatting and proof reading. Using this free service, authors can make their results available to the community, in citable form, before we publish the edited article. We will replace this *Accepted Manuscript* with the edited and formatted *Advance Article* as soon as it is available.

You can find more information about *Accepted Manuscripts* in the [Information for Authors](#).

Please note that technical editing may introduce minor changes to the text and/or graphics, which may alter content. The journal's standard [Terms & Conditions](#) and the [Ethical guidelines](#) still apply. In no event shall the Royal Society of Chemistry be held responsible for any errors or omissions in this *Accepted Manuscript* or any consequences arising from the use of any information it contains.

ARTICLE

Dehydrogenation of Ammonia-Borane by Cationic Pd(II) and Ni(II) Complexes in Nitromethane Medium: Hydrogen Release and Spent Fuel Characterization

Cite this: DOI: 10.1039/x0xx00000x

Received 00th January 2012,
Accepted 00th January 2012

DOI: 10.1039/x0xx00000x

www.rsc.org/

Sung-Kwan Kim,^a Sung-Ahn Hong,^a Ho-Jin Son,^{*a} Won-Sik Han,^d Artur Michalak,^c Son-Jong Hwang,^{*b} and Sang Ook Kang^{*a}

A highly electrophilic cationic Pd^{II} complex, [Pd(MeCN)₄][BF₄]₂ (**1**), bring about the preferential activation of the B–H bond in ammonia-borane (NH₃•BH₃, AB). At room temperature, the reaction between **1** in CH₃NO₂ and AB in tetraglyme leads to Pd nanoparticles and formation of spent fuels of the general formula MeNH_xBO_y as reaction byproducts, while 2 equiv of H₂ is efficiently released per AB equiv at room temperature within 60 seconds. For a mechanistic understanding of dehydrogenation by **1**, the chemical structure of spent fuels were intensely characterized through a series of analyses such as elemental analysis (EA), X-ray photoelectron spectroscopy (XPS), solid state magic-angle-spinning (MAS) NMR spectra (²H, ¹³C, ¹⁵N, and ¹¹B), and cross polarization (CP) MAS methods. During AB dehydrogenation, the involvement of MeNO₂ in the spent fuels showed that the mechanism of dehydrogenation catalyzed by **1** is different from that that found in previously reported results. This AB dehydrogenation derived from MeNO₂ is supported by a subsequent digestion experiment of AB spent fuel: B(OMe)₃ and *N*-methylhydroxylamine ([Me(OH)N]₂CH₂), which are formed from the methanolysis of AB spent fuel (MeNH_xBO_y), were identified by means of ¹¹B NMR and single crystal structural analysis, respectively. Similar catalytic behavior was also observed in AB dehydrogenation catalyzed by a nickel catalyst, [Ni(MeCN)₆][BF₄]₂ (**2**).

Introduction

Effective storage and release of hydrogen are very important for practical applications of hydrogen fuel-cell vehicle.^{1–3} Ammonia borane (NH₃BH₃, AB) has received considerable attention as an outstanding candidate for chemical hydrogen storage due to its low thermolysis temperature,⁴ high gravimetric storage density, high stability under normal fuel cell operating conditions, non-toxicity,^{5–7} and recently realized regeneration from spent fuel.⁸ Total hydrogen content of AB is 19.6 wt%, or 6.5 and 13.1 wt% for the first and second equivalent of hydrogen released, respectively, potentially securing to meet the ultimate targets of the DOE (7.5 system wt%).⁹ A high-performance dehydrogenation catalyst that can facilitate the fast yet efficient release of hydrogen at low temperatures is highly needed for the development of efficient on-board hydrogen storage materials based on AB. In this respect, several types of dehydrogenation catalysts have been developed, where H₂ evolution is mainly catalyzed by a wide range of homogeneous transition metal catalysts, such as rare transition metal catalysts (ruthenium,¹⁰ rhodium,¹¹ and iridium¹²) as well as more abundant metals such as group 4 organometallics,¹³ nickel,¹⁴ iron,¹⁵ and group 6 metal carbonyls.¹⁶ Group 10 transition metal complexes have been also exploited to achieve this target: only few results are represented by the Ni⁰-Enders³NHC (1,3,4-triphenyl-4,5-dihydro-1H-1,2,4-triazol-5-ylidene) complex,^{14,17} and nanostructured Pd⁰ heterogeneous systems¹⁸ that release 2~2.5 equivalents of hydrogen from AB.

Recently, we have reported dehydrogenation kinetics by the Pd^{II} complex [Pd(MeCN)₄][BF₄]₂ (**1**) with a 2.0 equiv H₂ release at room temperature within 60 seconds.¹⁹ However, in comparison with the rapidly growing number of catalysts, the amount of experimental studies that deal with mechanistic details is still limited.

With this in mind, we present a comprehensive experimental study about the mechanism of AB dehydrogenation with [Pd(MeCN)₄][BF₄]₂ (**1**) catalyst, which exhibited quite high activity (releasing more than 2 equiv of H₂) in our previous report.¹⁹ In addition to imparting the efficient dehydrogenation ability of **1**, we discovered that the dehydropolymerization forms mostly B–B bonds in a less regular process with preferential activation of B–H bond, but did not further investigate the structural elucidation of spent fuel for mechanism analysis in a recent preliminary communication.¹⁹ We initially thought that the composition of the dehydropolymerized product could be similar to other reported AB spent fuels ([H₂NB]_n).^{10,14} To our surprise, it is observed via solid state NMR analysis that there exists a sizable amount of carbon and oxygen in spent fuel besides B and N, indicating that C and O atoms are incorporated from the solvent used during AB dehydrogenation or external environment such as H₂O (in air) after AB dehydrogenation—albeit, to a much lesser extent than solvent. For this reason, we sought other explanations. In an effort to follow a mechanistic pathway of dehydrogenation, the spent fuels, which are solid residues precipitated after AB dehydrogenation, were characterized in detail by the solid state magic-angle-spinning

(MAS) NMR spectroscopy (^2H , ^{13}C , ^{15}N , and ^{11}B) and cross polarization (CP) magic angle spinning NMR. A subsequent digestion step of the spent fuel by methanolysis enabled their exact chemical species to be characterized by typical characterization tools such as single crystal X-ray and NMR analysis. On the basis of such analyses, it is rationalized that MeNO_2 is used as main source of carbon and oxygen in the spent fuel network, and its origin is clearly confirmed with a mechanistic study of deuterium tracing (^2H MAS NMR). In addition, to explore the generality of this mechanistic pathway, AB dehydrogenation by a nickel catalyst, $[\text{Ni}(\text{MeCN})_6][\text{BF}_4]_2$ (**2**) was performed. Compared to the palladium catalyst, the nickel catalyst (**2**) was less active in AB dehydrogenation only releasing 1.8 equiv of H_2 at 80 °C over the extended periods (60 minutes). Both palladium (**1**) and nickel (**2**) catalysts are believed to participate in the reaction with the same dehydrogenation sequence to produce similar spent fuels, borates. Herein, the results of the mechanistic studies of those reactions are presented.

Experimental Section

Materials and Methods. All of the experiments were carried out under a nitrogen atmosphere using the Schlenk techniques or in a Vacuum Atmosphere HE-493 drybox. The solvents were dried over Na (tetraglyme), Na/benzophenone (THF), CaCl_2 (nitromethane), and CaH_2 (methanol) distilled under nitrogen and deoxygenated prior to use. The deuterated solvents were dried through trap to trap distillation from CD_3NO_2 (CaCl_2), Na (C_6D_6) and CaH_2 (CD_3Cl , CD_3OD) and deoxygenated using three freeze-pump-thaw cycles. A palladium sponge and nitrosonium tetrafluoroborate were purchased from Strem chemicals. Catalysts **1** and **2** were prepared as described in the literature.²⁰

Analytical Methods. The solution NMR spectra were collected at room temperature using a Varian Mercury-300BB spectrometer unless otherwise stated. The ^{11}B NMR spectra were referenced to an external sample of $\text{BF}_3 \cdot \text{Et}_2\text{O}$ set to 0 ppm. For solid state MAS NMR spectroscopy, the samples were packed under an Ar gas atmosphere into a 4 mm ZrO_2 rotor that was sealed with a tight fitting Kel-F cap inside of a glovebox. The spectra were recorded using a Bruker DSX-500 spectrometer and a boron-free 4mm Bruker CPMAS probe. Sample spinning was performed using dry N_2 gas. The spectral frequencies were 500.23, 160.5, 50.7, and 76.8 MHz for ^1H , ^{11}B , ^{15}N , and ^2H nuclei, respectively. One dimensional ^{11}B MAS spectra were recorded after a 0.5 μs pulse ($< \pi/12$) with application of strong ^1H decoupling pulse. ^{11}B multiple-quantum (MQ) MAS NMR spectra were acquired employing the standard Z-filtered scheme²¹ and presented after the shearing transformation.²² Spectral decomposition and fittings were performed using Quasar routine in the DMFIT²³ software. The IR spectra were recorded on a Nicolet Avatar 330 FT-IR spectrometer with a KBr pellet. The elemental analyses were performed using a CE Instruments/Thermo Quest Italia Flash EA 1112 Series. Inductively coupled plasma-atomic emission spectroscopy was performed using a Varian 710-ES Model.

The spent fuel solid samples were analyzed using field-emission transmission electron microscopy (TEM, FEI TECNAI G2 200 kV and Jeol JEM 2100F), electron diffraction (ED), and energy-dispersive X-ray fluorescence spectroscopy (EDX). The X-ray diffraction (XRD) patterns were obtained using the 8C2 and 3C2 beam lines of the Pohang Light Source (PLS) with monochromatic radiation ($\lambda = 1.54520 \text{ \AA}$). X-ray photoelectron spectroscopy (XPS) was carried out using the 8A1 beam line of the Pohang Light Source

(PLS) and a laboratory-based spectrometer (VG Scientifics ESCALAB 250) with a photon energy of 1486.6 eV ($\text{Al K}\alpha$).

The quadrupole mass spectroscopy (QMS) data were obtained using a SRS (Stanford Research Systems) RGA200 quadrupole mass spectrometer that was attached to a glass vacuum line system.

A Quattro Micro triple quadrupole instrument that was equipped with an electrospray ionization source (Waters Corporation, Milford, MA, USA) was used in the negative and positive ionization mode. The sample solution was directly infused at a flow rate of 100 $\mu\text{L}/\text{min}$ using a syringe pump. The scanning mass range of the mass spectrometer was 5–2000 Da at a step size of 0.5 Da. The capillary voltage and the cone voltage were set at 3200 V and 15–25 V, respectively with nitrogen as the drying gas. The desolvation gas flow was 350 L/h and the cone gas flow was 70 L/h. The desolvation temperature was 350 °C and the source temperature was 100 °C.

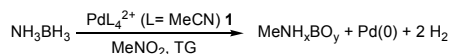
General Procedure of the AB Dehydrogenation

Apparatus and procedure for the Pd(II) catalyzed dehydrogenation. The reactor consisted of modified 50 mL double jacket glassware. A three way connector was modified to purge the system with argon gas and allowed the hydrogen gas that was produced during the reaction to pass through the mass flow meter. This system enabled the catalyst to be injected into the reactor without exposing the reactants to air. The reaction temperature was monitored and controlled using a thermocouple and an external heater/cooler, respectively. The experimental procedure involved filling the reactor with 2 mL of the tetraglyme solution containing 1.46 mmol of AB. The reactor was subsequently flush with argon for at least 30 min in order to minimize the moisture level inside the vessel. After the thermal equilibration between the reactor and the cold trap, 3 mol% of catalyst **1** was dissolved in 0.5 mL nitromethane (MeNO_2) and injected into the AB solution. The reaction time was calculated from the time when the catalyst was introduced into the mixture. The progress of the reaction was monitored by examining the amount of hydrogen that was generated using a volumetric technique, which was used for the real time tracking of the reaction. MeNO_2 (bp 101 °C) or other volatiles including NH_3 in the product stream were anticipated because of the large exotherm under the experimental conditions even though the temperature was controlled at 25 °C. In the apparatus setup, a $-90 \text{ }^\circ\text{C}$ cold bath (liquid N_2 with CH_2Cl_2) trapped the volatiles to ensure that the volume that was measured through the mass flow meter was only due to hydrogen. After the dehydrogenation, the solid was collected through filtration, rinsed with Et_2O and dried in vacuo. The possibility of a heterogeneous pathway was examined either by the supplemental addition of AB after dehydrogenation or mercury poisoning because of the fast hydrogen release kinetics for **1**. Both experiments indicate the presence of homogeneous catalysis: these successive dehydrogenations with a second charge of AB are slowed due to consumption and partial decomposition (to $\text{Pd}(0)$) of **1** during this catalytic reaction.^{11c}

Results and Discussions

Catalytic dehydrogenation of AB in tetraglyme with $[\text{Pd}(\text{MeCN})_4][\text{BF}_4]_2$ (1**) in MeNO_2 and characterization of spent fuels.**

Scheme 1. Formation of AB Dehydrocoupling Products (MeNH_xBO_y) with $[\text{Pd}(\text{MeCN})_4][\text{BF}_4]_2$ (1**) Catalyst**



It has been a general notion that coordinating solvent must be avoided due to the electrophilic nature of the cationic catalyst center. For this reason, MeCN was not considered as an appropriate solvent in the first place. In our earlier report, MeNO₂ is used as a solvent for dissolving **1** because **1** with weakly coordinating acetonitrile ligands is only stable in non-coordinating high polar solvent and insoluble in most organic solvents except for MeCN.¹⁹ Before AB dehydrogenation, we checked that **1** is stable and unreactive in MeNO₂: neither **1** nor AB was reactive with MeNO₂ at room temperature. Only when these three reagents were brought together, notable dehydrogenation occurred. When 3 mol% of **1** in MeNO₂ solution was added to a stirred tetraglyme solution containing AB at 25 °C, a vigorous hydrogen evolution with a typical strong exotherm was observed, resulting in 2.0 equiv of H₂ release within 60 s. During AB dehydrogenation, insoluble by-products were co-precipitated with Pd particles from the MeNO₂ and tetraglyme solution. The insoluble spent fuel was subsequently characterized as the preliminary composition of B_{1.00}C_{1.09}N_{0.95}H_{4.50}Pd_{0.024} through inductively coupled plasma (ICP)/elemental analysis (EA), and as B_{1.00}C_{1.40}N_{0.65}O_{1.89}Pd_{0.05} by X-ray photoelectron spectroscopy (XPS) (see Table 1 and Fig. S1). From these analyses, we found that a significant amount of carbon and oxygen was incorporated into the BNH_x matrix: an expected chemical composition in spent fuels that is comparable with those of original boron and nitrogen. Further structural characterization by the infrared (IR) spectrum revealed the preferential activation of B–H bonds. As shown in Fig. S2, the characteristic B–H peaks at around 2300 cm⁻¹ in AB have disappeared completely, indicating the preferential B–H activation mechanism.

Table 1 Elemental analysis and formula of spent fuel

Method	Spent fuel components						Formula of spent fuel
	B	C	N	O	H	Pd	
EA ^a	-	1.09	0.95	-	4.50	-	B _{1.00} C _{1.09} N _{0.95} H _{4.50} Pd _{0.024}
ICP ^b	1.00	-	-	-	-	0.024	
XPS ^c	1.00	1.40	0.65	1.89	-	0.05	

^aElemental analysis, ^bInductively coupled plasma-atomic emission spectroscopy, ^cX-ray photoelectron spectroscopy

Fig. 1 and Table 2 present high resolution solid state ¹¹B MAS NMR, 2D multiple quantum (MQ) MAS NMR spectra of the spent fuels, and ¹¹B peaks from the decomposition of 1D MAS NMR spectra, respectively. 2D-¹¹B MQMAS NMR spectrum was obtained to sort out the inequivalent boron sites that are indistinguishable in the 1D MAS spectrum. Two groups of peaks were initially sorted out by this method. The broad peaks between 10 and 20 ppm originate from boron atoms in trigonal geometry of BO₃ unit while several sharp peaks in the 6 to -6 ppm range were due to boron atoms in tetrahedral coordination. These *sp*³ are believed to be responsible for tetragonal BO₄ units. Based on the 2D MQMAS spectrum, the 1D spectrum was decomposed to 7 different sites as shown in Fig. 1. The peaks are compiled in Table 2. Note that additional resonance is seen at -10 ppm (see the 2D spectrum) but was ignored due to its negligible contribution. 1D ¹¹B MAS spectrum without ¹H decoupling allowed us to conclude that nearly all boron peaks except the peak at -6 ppm (and -10 ppm) are without direct B–H bonds. However, those peaks showed high efficiency (intensity) in ¹H-¹¹B cross polarization MAS NMR (see Fig. 1), indicating that boron atoms are in close proximity to either NH or -CH organic species. The ratio of [B]_{trigonal} vs [B]_{tetrahedral} (B³:B⁴) was calculated to be 2:3 from the spectral decomposition, which allows speculation about a possible structure. Lastly, the fairly sharp peak at -1.6 ppm is believed to be BF₄⁻ although its binding

cation is not known. As shown in Table 2, ¹¹B NMR of AB spent fuel showed a mixture of two trigonally (*sp*²) and tetrahedrally (*sp*³) coordinated boron atoms. The trigonal boron atoms are clearly distinctive from those of BN₃, BN₂H type of *sp*² boron sites of polyborazylene, or BN²⁴ in comparison with simulated spectra of BN, BN₂H, and B(OH)₃, which are plotted together with experimental data (see Fig. 1 and S2).

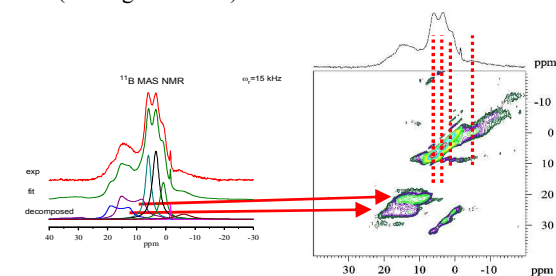


Fig. 1 1D ¹¹B MAS (left) and 2D ¹¹B MQMAS (right) NMR spectra of the spent fuel.

Table 2 ¹¹B peaks from deconvolution of 1D and 2D MAS NMR spectra

Chemical shift (δ _{iso})	C _Q (MHz) ^a	η	Relative intensity ratio
21.9	2.53	0.1	0.13
18.5	2.70	0.1	
6.2	0.5	1	0.20
3.6	0.5	1	
1.1	0.5	1	
-6.0	0.5	1	0.04
-1.6	-	-	<0.01

^aC_Q: quadrupole coupling constant (= e²qQ/h); η: asymmetry parameter (= (V_{xx}-V_{yy})/V_{zz}), where their usual definition can be readily found for quadrupole interaction in magnetic resonance²⁵

In addition to the routine probing nuclei such as ¹H and ¹¹B, the chemical transformation of B–N bond of AB was further explored by ¹⁵N NMR spectroscopy. The ¹⁵N labelled AB²⁷ was used for this purpose and the same catalytic reaction was performed using the Pd catalyst and the spent fuel under the same condition that has been used in the un-labelled AB case (see above). The corresponding ¹⁵N MAS and CPMAS NMR spectra of ¹⁵N-sfAB sample are shown in Fig. 2-

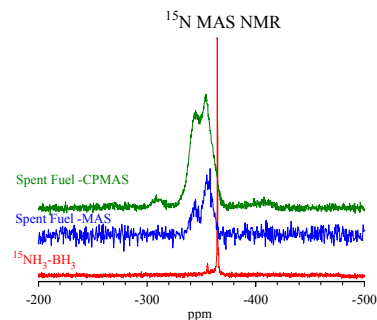


Fig. 2 ¹⁵N MAS and CPMAS NMR spectra of sfAB that was generated using ¹⁵N labelled AB (¹⁵NH₃-BH₃). Note the vertical scale of ¹⁵NH₃-BH₃ was adjusted by 1/100 for comparison purpose. The ¹⁵N shift was externally referenced to neat CH₃NO₂.

¹⁵N signal of the remaining nitrogen compound in the spent fuel showed two major peaks at -340.5 and -353 ppm with the intensity

ratio of 1:3. While the signal by MAS alone is weak and a time-consuming experiment to obtain spectrum with good signal to noise ratio due to long relaxation time and low nitrogen quantity, ^1H - ^{15}N cross polarization (CP) method appears to improve the signal quality markedly and more detailed spectral analysis was possible. The CPMAS method made the small and broad resonances at -310 and -410 ppm, which were invisible in the MAS spectrum. Typically peaks in -250 and -330 ppm range represent nitrogen atoms that are trigonally coordinated while those in the $-330 \sim -400$ ppm range are attributed with N atoms in tetrahedrally coordination.²⁶ According to Gervais *et al.* and references cited, NB_3 sites appear between $-250 \sim -300$ ppm. As shown in Fig. 2, besides the small peak near at -310 ppm, most of N containing species of sfAB can be associated with tetrahedrally coordinated N sites that are typically found in PAB ($-\text{NH}_2\text{BH}_2$).²⁷ The corresponding ^{11}B signal, tetrahedrally coordinated B sites and especially those peaks at ~ -10 ppm, explains the remaining B-N moieties in the spent fuel. The -310 ppm peak might show the presence of B_2NH trigonal sites in a hexagonal ring structure as shown here. Note, however, that among the ^{15}N signal, its contribution is negligibly small. It is not yet clear about a possible local structure of N sites that could represent the -410 ppm peak. Again, its contribution is negligible.

Catalytic dehydrogenation of AB in tetraglyme with **1** in MeNO_2-d_3 and characterization of spent fuels.

In an effort to elucidate the incorporation of MeNO_2 into spent fuel framework, an experiment using deuterium tracing was performed via ^2H MAS NMR analysis with MeNO_2-d_3 (CD_3NO_2) employed as solvent to dissolve **1**. As soon as 3 mol% of **1** dissolved in MeNO_2-d_3 was added to a stirred tetraglyme solution containing AB at 25°C , fast AB dehydrogenation was observed as expected, completing a 2.0 equiv H_2 release in 60 s. The dehydrogenated products were co-precipitated with Pd particles from the MeNO_2-d_3 and tetraglyme solution.

Structural characterization of the precipitant is obtained by ^2H MAS NMR analysis. The majority of signal is due to $-\text{CD}_3$ moiety showing C_3 free rotational motion, indicated by the quadrupole coupling constant ($C_q = 54$ kHz) determined from a spectral fit of the experimental spectrum (see Fig. 3a), and this could be bound to the boron compounds via reduced NO_2 group. It is observed that there exist three different deuterium species: besides the CD_3 - at 0.4 ppm ($C_q = 54$ kHz, dominating > 70%), there are CD- group (immobile, 5.7 ppm, $C_q = 171.4$ kHz, 17%) and solvent like mobile CD_3NO_2 phase (4.8 ppm, $C_q = 10$ kHz, 12%, see Fig. 3b).

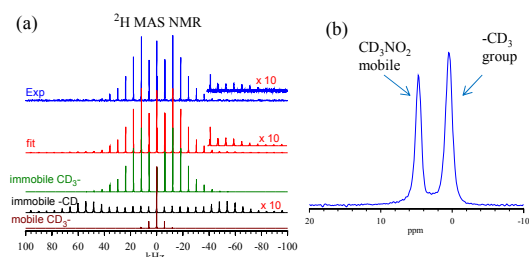


Fig. 3 ^2H MAS NMR of the spent fuel from dehydrogenation of AB in tetraglyme by **1** in MeNO_2-d_3 , (a) experimental ^2H MAS spectrum at a spinning rate of 6 kHz, a fitted spectrum, and the corresponding 3 components, (b) the center band. The presence of immobile C-D group is manifested by a powder pattern (see $\times 10$ scaled portion) of a typical C-D quadrupole interaction ($C_q=171.4$ kHz). The shift in ppm was referenced to D_2O at 4.7 ppm.

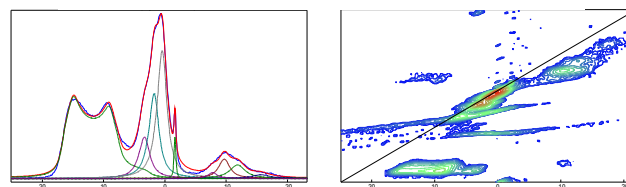


Fig. 4 1D ^{11}B MAS (left) and 2D ^{11}B MQMAS (right) NMR spectra of spent fuels from dehydrogenation of AB in tetraglyme by **1** in MeNO_2-d_3 .

In high resolution solid state ^{11}B MAS NMR analysis, we found that peaks of the MeNO_2-d_3 mediated AB spent fuel are similar to those of non-deuterated solvent system, which is described in earlier discussion part (Fig. 1 and Table 2), showing identical kinetics of deuterated and non-deuterated MeNO_2 solvent system. ^{11}B peaks from decomposition of 1D and 2D MAS NMR spectra is summarized in Table 3. As shown in Fig. 4, 1D ^{11}B MAS NMR spectra clearly shows the simplest and clean line shape of the BO_3 units at around 18 ppm. The Q_{cc} and eta parameters are classified into two different kinds of families. Several sharp peaks in the $4 \sim -2$ ppm range are for borons in tetrahedral coordination, which are believed to be responsible for tetragonal BO_4 units. The broad peak at $-8 \sim -16$ ppm is assigned as a possible location for BH_2 units, implying the incomplete dehydrogenation.

The reactivity of AB with MeNO_2 and characterization of spent fuels.

For the insight of the cross reactivity between AB and MeNO_2 , AB dehydrogenation by MeNO_2 is performed without Pd catalyst **1** and tetraglyme solvent. We observed trace amount of released gas over the extended periods (10 h at 25°C). We tested the MeNO_2 -mediated performance, plotting the amount of H_2 released with different reaction temperature ($25, 60, 80,$ and 100°C). Up to 60°C , no discernible H_2 production was noted, but observed in 80°C to 100°C temperature is the detectable dehydrogenation with white precipitations, which are insoluble in most aprotic solvents.

Table 3 ^{11}B peaks from decomposition of 1D and 2D MAS NMR spectra

shift	Q_{cc} (MHz)	eta	rel Int ratio	
18.01	2.52	0.1	0.45	sp^2
3.62	0.5	1	0.08	sp^3
2.05	0.5	1	0.14	
0.74	0.5	1	0.22	
-1.62	0.2	1	0.04	
-7.5	0.5	1	0.01	
-9.44	0.5	1	0.01	
-11.57	0.5	1	0.01	
-15.4	0.5	1	0.04	

Table 4 ^{11}B peaks from decomposition of 1D and 2D MAS NMR spectra

shift (ppm)	Q_{cc} (MHz)	eta	rel int ratio
21.9	2.53	0.15	0.03
17.91	2.52	0.15	0.30
11.31	0.5	1	0.01
9.14	0.5	1	0.02
6.69	0.5	1	0.11
3.26	0.5	1	0.25
0.78	05	1	0.10

Journal Name

-7.02	0.5	1	0.03
-10.37	0.5	1	0.08
-13.84	0.5	1	0.06

The precipitates (S1) produced from AB dehydrogenation without **1** and tetraglyme is also characterized by ^1H and ^{11}B MAS NMR analysis. For the exact comparison, it is compared with NMR spectra of both the AB spent fuels ($[\text{CNH}_x]\text{BO}_y$), which are generated with **1** and tetraglyme in CH_3NO_2 solvent, and precipitates (S2) generated with **1** in CD_3NO_2 solvent (see Fig. 5). Overall the outcome of both ^1H and ^{11}B MAS NMR spectra for S1 is noticeably different from those of BNHx. However, the difference is mainly due to the degree of reaction progressed in S1, which was supposedly lower due to the lack of the catalyst **1**. The S2 shows simply only one BO_3 peak at 18.4 ppm. The S1 shows the same BO_3 peak with very small addition of the secondary BO_3 peak at 21.6 ppm (see Table 4). Interestingly, the S1 contains numerous BO_4 covering wide range from -4 ppm to 6 ppm, seemingly the BO_4 peaks seen for both $[\text{CNH}_x]\text{BO}_y$ and S2 (see Fig. 5). The BH_2^- units at -10 ppm²⁸ are seen for both S1 and S2 in relatively high concentration, showing the incomplete dehydrogenation. These results strongly support the involvement of CH_3NO_2 in AB spent fuels.

Catalytic dehydrogenation of AB in tetraglyme with $[\text{Ni}(\text{MeCN})_6][\text{BF}_4]_2$ (**2**) in MeNO_2 and characterization of spent fuels.

AB dehydrogenation was performed using the $[\text{Ni}(\text{MeCN})_6][\text{BF}_4]_2$ (**2**) under the same stated conditions. However, Ni catalyst **2** was inactive under mild conditions, only producing 0.2 and 1.0 equiv of H_2 (in 2 h) at 25 and 60 °C, respectively. At a slightly increased temperature, 80 °C, 1.8 equiv of H_2 is released during 60 min. (see Fig. 6). Similar to the typical method mentioned above, 3 mol% of **2**, which is dissolved in 0.5 mL of MeNO_2 , was added to 2 mL of a stirred tetraglyme solution containing 0.045 g (1.46 mmol) of AB at different temperatures. The dehydrogenation product is co-precipitated with Ni particles completely from tetraglyme and MeNO_2 , which were later found to be insoluble in most aprotic solvents. Except for the dehydrogenation performance, the signs of a reaction including production of precipitation are similar to the case of Pd catalyst **1**.

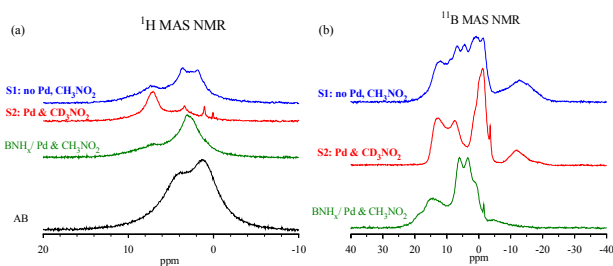
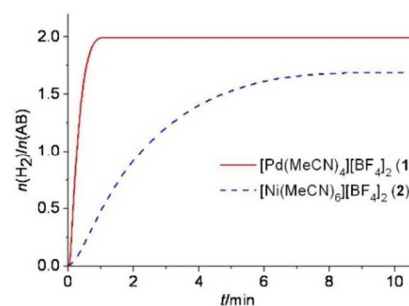


Fig. 5 (a) ^1H and (b) ^{11}B MAS NMR spectra comparison for white precipitations of AB spent fuel with MeNO_2 solvent.

^{11}B MAS NMR spectra of spent fuel produced by **2** in MeNO_2 reveals very similar features to that from **1** as described in Table 5 and Fig. 7. Two groups of peaks were initially sorted out by this method. The broad peaks between 10 and 20 ppm are apparently assigned as boron atoms in trigonal geometry of BO_3 units, while several sharp peaks ranging from 6 to -6 ppm can be assigned as boron atoms in a tetrahedral coordination. These sp^3 are believed to

be responsible for tetragonal BO_4 units. Similar to those found in S1 and S2 case, the broad peaks at -10 ~ -15 ppm are assigned as a possible location for BH_2^- , which means the incomplete dehydrogenation derived from the relatively low catalytic ability of



Ni catalyst **2**. Based on the 2D spectrum, the 1D spectrum was decomposed to 8 different sites as shown in Table 5. The ratio of $[\text{B}]_{\text{trigonal}}:[\text{B}]_{\text{tetrahedral}} (sp^2:sp^3)$ was calculated to be 2:3 from the spectral decomposition. Consequently, this spectral similarity in solid NMR spectra (of spent fuels by **1** and **2**) elucidates a mechanism for the MeNO_2 -mediated AB dehydrogenation.

Fig. 6 AB dehydrogenation kinetic profiles for $[\text{Pd}(\text{MeCN})_4][\text{BF}_4]_2$ (**1**) at 25 °C in MeNO_2 and $[\text{Ni}(\text{MeCN})_6][\text{BF}_4]_2$ (**2**) in MeNO_2 at 80 °C.

Table 5. ^{11}B peaks from decomposition of 1D and 2D MAS NMR spectra

Chemical shift (δ_{iso})	C_Q	Relative Intensity ratio	
21.8	2.6	0.11	sp^2 : 0.41
18.4	2.53	0.30	
9.39	0.2	0.04	sp^3 : 0.59
6.55	0.2	0.04	
3.57	0.2	0.23	
0.8	0.5	0.16	
-10.08	0.2	0.07	
-14.94	0.2	0.06	

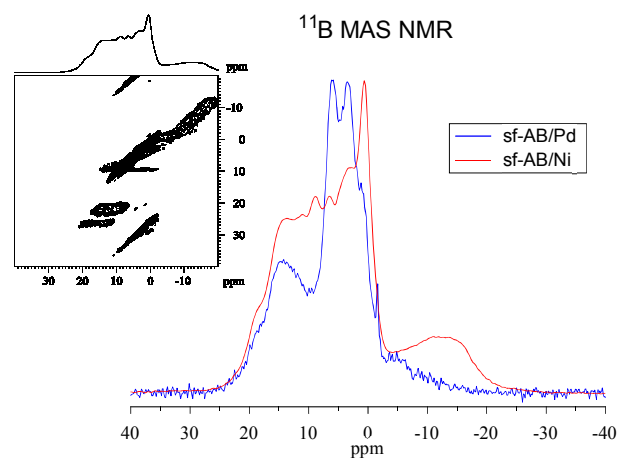
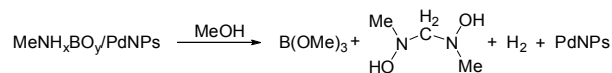


Fig. 7 Comparison of 1D ^{11}B MAS and 2D ^{11}B MQMAS (inset) NMR spectra of spent fuels produced by **1** and **2** catalysts in MeNO_2 /tetraglyme solution.

Structural characterization through digestion of the spent fuels: Pd-NPs catalyzed methanolysis of MeNH_xBO_y .



In an effort to analyze the exact chemical species of the spent fuel remaining after AB dehydrogenation, the spent fuel was digested by adding methanol. Digestion of spent fuel is proceeded with addition of methanol. Generally Pd nanoparticles have been well known as an effective catalyst for the dehydrogenative methanolysis of AB,²⁹ and thus the spent fuel (MeNH_xBO_y/PdNPs) is used for the impromptu digestion without doing any treatment except subsequent addition of methanol. All by-products (including releasing gas) generated after the digestion step were fully characterized by NMR, quadrupole mass spectroscopy (QMS), and single crystal X-ray analysis. The ¹¹B NMR chemical shift of 18.1 ppm indicates the formation of B(OMe)₃ from the digestion (see Fig. S4 in Supporting Information). The spent fuel containing the Pd nanoparticles, MeNH_xBO_y/PdNPs (1.07 g, 40 mmol) was placed in a two-neck round-bottom flask that was fitted with a septum inlet and a reflux condenser with a connecting tube. The connecting tube is attached to the mass flow meter via a gas bubbler containing 100 mL of water in order to trap the ammonia gas. Gas evolution was detected when methanol (12 mL, 296 mmol) was added to the spent fuel under an argon atmosphere. The released gas was transferred to a QMS that was directly connected to the vacuum line in order to identify the gaseous by-product. Fig. 8 clearly shows the gas that was released after the addition of methanol solvent is mostly hydrogen. When the hydrogen evolution ceased (64 mL, 2.05 mmol), the aqueous solution of ammonia from the trap was titrated against standard 0.1 N aq HCl. Only a trace amount of NH₃ was estimated to be 0.0017 g (0.1 mmol). At the end of the reaction, the black solids (0.06 g, 0.563 mmol) were collected through filtration. The presence of PdNPs was confirmed by the XRD analysis in Fig. 9a. Methanol and B(OMe)₃ were recovered from distillation of the filtrate at 69 °C. The ¹¹B NMR spectrum of filtrate clearly shows the exclusive formation of B(OMe)₃. Subsequent isolation of B(OMe)₃ (1.3 g, 12.51 mmol) from the residue was performed through the trap to trap fractionation under high vacuum (10⁻⁸ torr) at -30 °C. To analyze the exact composition of the final by-products remaining after isolation of B(OMe)₃, the non-volatile and viscous residue was recrystallized from methanol solution. From X-ray structural study of the obtained crystal sample, we realized the exact chemical structure of residue is *N,N'*-dihydroxy-*N,N'*-dimethylmethanediamine ([Me(OH)N]₂CH₂) (0.663 g, 6.255 mmol) and they exist as a single product (see Fig. 9b). Consequently, through this digestion experiment of dehydrogenated products and their further characterization, it is reconfirmed that the AB dehydrogenation by **1** is performed through a MeNO₂ solvent-mediated mechanism and the involvement of the polar solvent in this catalytic reaction is a key step for AB dehydrogenation.

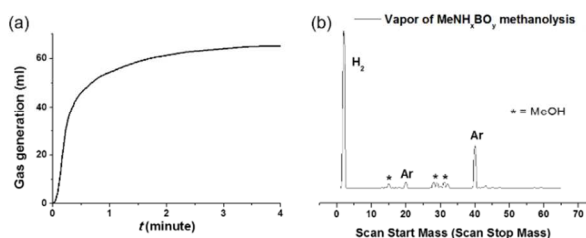


Fig. 8 (a) H₂ release kinetic profile for the digestion of the spent fuel with the PdNPs and (b) mass spectrum of the volatiles produced from the MeNH_xBO_y methanolysis with the PdNPs. The most intensive mass number detected was *m/z* = 2 (H₂).

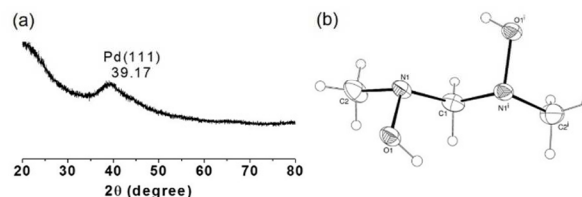


Fig. 9 (a) XRD patterns of the recovered Pd particles from the methanolysis and (b) ORTEP drawing of the molecular structure of [Me(OH)N]₂CH₂.

Conclusion

In summary, we have demonstrated that the mechanistic study of AB dehydrogenation by a highly electrophilic cationic Pd^{II} complex (**1**) with structural elucidation of spent fuels. To understand the exact mechanistic pathway, the chemical structure of the spent fuels was fully characterized by solid state magic-angle-spinning (MAS) NMR spectra (²H, ¹³C, ¹⁵N, and ¹¹B) and cross polarization magic angle spinning (CPMAS). From a series of NMR analyses with a deuterium tracing study (CD₃NO₂), we reasoned that the carbon and oxygen species of MeNO₂, which is used as solvent to dissolve **1**, are significantly involved in formation of spent fuel, MeNH_xBO_y. Two B(OMe)₃ and [Me(OH)N]₂CH₂ species, which is produced by methanolysis (digestion step) of MeNH_xBO_y, are clearly characterized by X-ray crystallography and NMR analysis, providing a direct evidence of carbon and oxygen incorporation in spent fuels. In addition, such a mechanism is further generalized by a nickel catalyst, [Ni(MeCN)₆][BF₄]₂ (**2**). This work offers the significance and criteria of non-coordinating polar solvent in the design and development of catalytic AB dehydrogenation systems. Efforts toward mechanistic investigations as well as performance optimization of AB catalytic system utilizing different types of polar solvent are currently underway.

Acknowledgements

This work was supported by a Korea University research grant 2014.

Notes and references

- ^a Department of Advanced Materials Chemistry, Korea University, Sejong 339-700, Korea. E-mail: hjson@korea.ac.kr; sangok@korea.ac.kr
^b Division of Chemistry and Chemical Engineering, California Institute of Technology, Pasadena, CA 91125, United States. Email: sonjong@cheme.caltech.edu
^c Department of Theoretical Chemistry, Faculty of Chemistry, Jagiellonian University, R. Ingardena 3, 30-060 Kraków, Poland.
^d Department of Chemistry, Seoul Women's University, Hwarang-ro 621, Seoul, Korea.

Electronic Supplementary Information (ESI) available: (S1 and S2) X-ray photoelectron spectroscopy (XPS) and IR spectra of spent fuel. (S3) ¹¹B MAS NMR spectrum of spent fuel. (S4) Digestion procedures of spent fuel. (S5 and S6) ¹³C MAS, CPMAS, 1D ¹¹B MAS, and 2D ¹¹B MQMAS NMR spectra of spent fuel. See DOI: 10.1039/b000000x/

1. U.S. DOE, "Hydrogen, Fuel Cells & Infrastructure Technologies Program" (<http://www.eere.energy.gov/hydrogenandfuelcells/storage>).
2. The American Physical Society, "The Hydrogen Initiative" (http://www.aps.org/public_affairs/index.cfm).
3. L. Schlapbach, A. Züttel, *Nature* 2001, **414**, 353.
4. F. Baitalow, J. Baumann, G. Wolf, K. Jaenicke-Rößler, G. Leitner, *Thermochim. Acta*, 2002, **391**, 159.
5. H. W. Langmi, G. S. McGrady, *Coord. Chem. Rev.*, 2007, **251**, 925.
6. C. W. Hamilton, R. T. Baker, A. Staubitz, I. Manners, *Chem. Soc. Rev.*, 2009, **38**, 279.
7. A. Staubitz, A. P. M. Robertson, I. Manners, *Chem. Rev.*, 2010, **110**, 4079.
8. (a) B. L. Davis, D. A. Dixon, E. B. Garner, J. C. Gordon, M. H. Matus, B. Scott, F. H. Stephens, *Angew. Chem., Int. Ed.*, 2009, **48**, 6812; (b) A. D. Sutton, B. L. Davis, K. X. Bhattacharyya, B. D. Ellis, J. C. Gordon, P. P. Power, *Chem. Commun.*, 2010, **46**, 148; (c) A. D. Sutton, A. K. Burrell, D. A. Dixon, E. B. Garner III, J. C. Gordon, T. Nakagawa, K. C. Ott, J. P. Robinson, M. Vasiliu, *Science*, 2011, **331**, 1426.
9. (a) J. Graetz, *Chem. Soc. Rev.*, 2009, **38**, 73; (b) Sigma-Aldrich "Material Matters" special issue 2007, Volume 2, Number 2, <http://www.scribd.com/doc/12703635/Hydrogen-Storage-Materials-Material-Matters-v2n2>.
10. (a) N. Blacquiere, S. Diallo-Garcia, S. I. Gorelsky, D. A. Black, K. Fagnou, *J. Am. Chem. Soc.*, 2008, **130**, 14034; (b) Käß, M.; Friedrich, A.; Drees, M.; Schneider, S. *Angew. Chem. Int. Ed.*, 2009, **48**, 905; (c) G. Alcaraz, S. Sabo-Etienne, *Angew. Chem., Int. Ed.*, 2010, **49**, 7170; (d) A. N. Marziale, A. Friedrich, I. Klopsch, M. Drees, V. R. Celinski, J. Schmedt auf der Günne, S. Schneider, *J. Am. Chem. Soc.*, 2013, **135**, 13342.
11. (a) Chen, Y.; Fulton, J. L.; Linehan, J. C.; Autrey, T. *J. Am. Chem. Soc.*, 2005, **127**, 3254; (b) Jaska, C. A.; Temple, K.; Lough, A. J.; Manners, I. *J. Am. Chem. Soc.*, 2003, **125**, 9424; (c) C. A. Jaska, I. Manners, *J. Am. Chem. Soc.*, 2004, **126**, 9776.
12. (a) Denney, M. C.; Pons, V.; Hebden, T. J.; Heinekey, M.; Goldberg, K. I. *J. Am. Chem. Soc.*, 2006, **128**, 12048; (b) A. Paul, C. B. Musgrave, *Angew. Chem., Int. Ed.*, 2007, **46**, 8153.
13. (a) T. J. Clark, C. A. Russell, I. Manners, *J. Am. Chem. Soc.*, 2006, **128**, 9582; (b) D. Pun, E. Lobkovsky, P. J. Chirik, *Chem. Commun.*, 2007, 3297; (c) M. E. Sloan, A. Staubitz, T. J. Clark, C. A. Russell, G. C. Lloyd-Jones, I. Manners, *J. Am. Chem. Soc.*, 2010, **132**, 3831; (d) T. Miyazaki, Y. Tanabe, M. Yuki, Y. Miyake, Y. Nishibayashi, *Organometallics*, 2011, **30**, 2394; (e) T. Beweries, J. Thomas, M. Klahn, D. Heller, A. Schulz, U. Rosenthal, *ChemCatChem*, 2011, **3**, 1865.
14. R. J. Keaton, J. M. Blacquiere, R. T. Baker, *J. Am. Chem. Soc.*, 2007, **129**, 1844.
15. (a) J. R. Vance, A. P. M. Robertson, K. Lee, I. Manners, *Chem. Eur. J.*, 2011, **17**, 4099; (b) R. T. Baker, J. C. Gordon, C. W. Hamilton, N. J. Henson, P.-H. Lin, S. Maguire, M. Murugesu, B. L. Scott, N. C. Smythe, *J. Am. Chem. Soc.*, 2012, **134**, 5598. (c) J. R. Vance, A. Schafer, A. P. M. Robertson, K. Lee, J. Turner, G. R. Whittell, I. Manners, *J. Am. Chem. Soc.*, 2014, **136**, 3048; (d) Sonnenberg, J. F.; Morris, R. H. *ACS Catal.*, 2013, **3**, 1092–1102. e) Bhattacharya, P.; Krause, J. A.; Guan, H. *J. Am. Chem. Soc.*, 2014, **136**, 11153.
16. Y. Kawano, M. Uruichi, M. Shimoi, S. Taki, T. Kawaguchi, T. Kakizawa, H. Ogino, *J. Am. Chem. Soc.*, 2009, **131**, 14946.
17. X. Yang, M. B. Hall, *J. Am. Chem. Soc.*, 2008, **130**, 1798.
18. (a) Ö. Metin, S. Duman, M. Dinç, S. Özkar, *J. Phys. Chem. C*, 2011, **115**, 10736; (b) R. P. Shrestha, H. V. K. Diyalanage, T. A. Semelsberger, K. C. Ott, A. K. Burrell, *Int. J. Hydrogen Energy*, 2009, **34**, 2616.
19. S. K. Kim, W.-S. Han, T.-J. Kim, T.-Y. Kim, S. W. Nam, M. Mitoraj, Ł. Piekoś, A. Michalak, S.-J. Hwang, S. O. Kang, *J. Am. Chem. Soc.*, 2010, **132**, 9954.
20. (a) R. F. Schramm, B. B. Wayland, *J. Chem. Soc. Chem. Commun.*, 1968, 898; (b) T. Lai, A. Sen, *Organometallics* 1984, **3**, 866.
21. J.-P. Amoureux, C. Fernandez, S. Steuernagel, *Journal of Magnetic Resonance, Series A*, 1996, **123**, 116.
22. J. P. Amoureux, M. Pruski, In: *Encyclopedia of NMR*, Ed. Grant, D.M.; Harris, R.K. Wiley, 2002, Vol 9, p 226.
23. D. Massiot, F. Fayon, M. Capron, I. King, S. Le Calvé, B. Alonso, J.-O. Durand, B. Bujoli, Z. Gan, G. Hoatson, *Magnetic Resonance in Chemistry*, 2002, **40**, 70.
24. (a) S. Mecking, *Coord. Chem. Rev.*, 2000, **203**, 325; (b) C. Gervais, J. Maquet, F. Babonneau, C. Duriez, E. Framery, M. Vaultier, P. Florian, D. Massiot, *Chem. Mater.*, 2001, **13**, 1700; (c) J. Li, S. Bernard, V. Salles, C. Gervais, P. Miele, *Chem. Mater.*, 2010, **22**, 2010; (d) C. Gervais, E. Framery, C. Duriez, J. Maquet, M. Vaultier, F. Babonneau, *J. Eur. Ceram. Soc.*, 2005, **25**, 129.
25. Freude, D.; Haase, J. Quadrupole effects in solid-state nuclear magnetic resonance. *NMR Basic Principles and Progress*, edited by P. Diehl, E. Fluck, H. Günther, R. Kasfeld, and J. Seelig, Springer-Verlag, Berlin 1993, **29**, 1.
26. C. Gervais, F. Babonneau, *J. Organomet. Chem.*, 2002, **657**, 75.
27. W. J. Shaw, J. C. Linehan, N. K. Szymczak, D. J. Heldebrant, C. Yonker, D. M. Camaioni, R. T. Baker, T. Autrey, *Angew. Chem. Int. Ed.*, 2008, **47**, 7493.
28. (a) A. C. Stowe, W. J. Shaw, J. C. Linehan, B. Schmid, T. Autrey, *Phys. Chem. Chem. Phys.*, 2007, **9**, 1831; (b) J. F. Kostka, R. Schellenberg, F. Baitalow, T. Smolinka, F. Mertens, *Eur. J. Inorg. Chem.*, 2012, 49.
29. H. Erdogan, Ö. Metin, S. Özkar, *Phys. Chem. Chem. Phys.*, 2009, **11**, 10519.